Micromagnetic stimulation (μMS) dose-response of the rat sciatic nerve

Journal of Neural Engineering

PAPER

Micromagnetic stimulation (μMS) dose-response of the rat sciatic nerve

Renata Saha[1], **Zachary Sanger**[2], **Robert P Bloom**[1], **Onri J Benally**[1], **Kai Wu**[1], **Denis Tonini**[1], **Walter C Low**[3,4,5], **Susan A Keirstead**[4,5], **Theoden I Netoff**[2] and **Jian-Ping Wang**[1,*]

[1] Department of Electrical and Computer Engineering, University of Minnesota, Minneapolis, MN, United States of America
[2] Department of Biomedical Engineering, University of Minnesota, Minneapolis, MN, United States of America
[3] Department of Neurosurgery, University of Minnesota, Minneapolis, MN, United States of America
[4] Stem Cell Institute, University of Minnesota, Minneapolis, MN, United States of America
[5] Department of Integrative Biology & Physiology, University of Minnesota, Minneapolis, MN, United States of America
[*] Author to whom any correspondence should be addressed.

E-mail: jpwang@umn.edu

Keywords: micromagnetic neurostimulation, dose-response relationship, microcoils, induced electric field, orientation-dependence, rat sciatic nerve, spatially-selective neuromodulation

Supplementary material for this article is available online

OPEN ACCESS

RECEIVED
22 October 2022

REVISED
20 April 2023

ACCEPTED FOR PUBLICATION
15 May 2023

PUBLISHED
31 May 2023

Abstract

Objective. The objective of this study was to investigate the effects of micromagnetic stimuli strength and frequency from the Magnetic Pen (MagPen) on the rat right sciatic nerve. The nerve's response was measured by recording muscle activity and movement of the right hind limb. *Approach.* The MagPen was custom-built to be stably held over the sciatic nerve. Rat leg muscle twitches were captured on video, and movements were extracted using image processing algorithms. EMG recordings were also used to measure muscle activity. *Main results.* The MagPen prototype, when driven by an alternating current, generates a time-varying magnetic field, which, according to Faraday's law of electromagnetic induction, induces an electric field for neuromodulation. The orientation-dependent spatial contour maps of the induced electric field from the MagPen prototype have been numerically simulated. Furthermore, in this *in vivo* work on μMS, a dose-response relationship has been reported by experimentally studying how varying the amplitude (Range: 25 m$V_{\text{p-p}}$ through 6 $V_{\text{p-p}}$) and frequency (range: 100 Hz through 5 kHz) of the MagPen stimuli alters hind limb movement. The primary highlight of this dose-response relationship (repeated over n rats, where $n = 7$) is that for a μMS stimuli of higher frequency, significantly smaller amplitudes can trigger hind limb muscle twitch. This frequency-dependent activation can be justified by Faraday's Law, which states that the magnitude of the induced electric field is directly proportional to the frequency. *Significance.* This work reports that μMS can successfully activate the sciatic nerve in a dose-dependent manner. The impact of this dose-response curve addresses the controversy in this research community about whether the stimulation from these μcoils arise from a thermal effect or micromagnetic stimulation. MagPen probes do not have a direct electrochemical interface with tissue and therefore do not experience electrode degradation, biofouling, and irreversible redox reactions like traditional direct contact electrodes. Magnetic fields from the μcoils create more precise activation than electrodes because they apply more focused and localized stimulation. Finally, unique features of μMS, such as the orientation dependence, directionality, and spatial specificity, have been discussed.

1. Introduction

Implantable neuromodulation devices have been used for the treatment of chronic pain [1–3], brain disorders [4–7] and have been applied as retinal [8, 9] and cochlear prostheses [8, 9]. The use of electric shock from Torpedo fish for the treatment of chronic pain dates back to the 15th century AD [10]. This practice was soon followed by reports of muscle contraction due to electrical stimulation [11, 12] in the 18th century. However, the modern era of neuromodulation for the treatment of chronic pain began in the 1960s [13]. *Sciatica* is a diagnostic condition where excruciating pain travels along the path of the sciatic nerve, which originates from the spinal cord and extends through the legs. Transcutaneous electric nerve stimulation [14, 15] has been proven to be quite effective for *sciatica* treatment, and percutaneous electric nerve stimulation is being investigated as a viable and possibly even better alternative [16, 17].

The spatially selective and directional activation of the peripheral nervous system (PNS) has been pursued for over two decades by peripheral nerve interface designers [18]. Of the electrodes that have been designed for the precise stimulation of the PNS, the transverse intrafascicular multi-electrode array (TIME) [19], the longitudinal intrafascicular electrode (LIFE) [20], the Cuff electrodes, and the Utah slanted electrode array (USEA) [21] deserve special mention. TIME, LIFE, and USEA are intrafascicular electrodes, which means they are surgically inserted to penetrate the peripheral nerve and provide microstimulation. Cuff electrodes provide extraneural activation, which means they wrap around the nerve, and it is impossible for the nerve to escape the Cuff electrode contact. While USEA electrodes have been recently reported as an advanced electrode array design, literature reports suggest that TIME is the only electrode that offers good neural stimulation selectivity at both the intra- and interfascicular level. LIFE allows enhanced selectivity on only the intrafascicular level, while multipolar Cuff electrodes offer selectivity on the interfascicular level. Despite the success of these peripheral nerve stimulators, the electrodes are in close galvanic contact with biological tissue, which can result in biofouling [22, 23]. Biofouling increases the voltage required to achieve the same field strength in tissue and can cause the field strength needed to activate tissue to exceed safe limits. Here, we present an implantable technology based on micromagnetic stimulation (μMS). It uses submillimeter-sized coils, or microcoils (μcoils), which, when driven by a time-varying current, generate a time-varying magnetic field. This magnetic field induces an electric field in the surrounding tissue according to Faraday's laws of electromagnetic induction. Because stimulation occurs through an inductive effect, the μcoils do not come in direct galvanic contact with the biological tissue. Therefore, these μcoils are invulnerable to biofouling, unlike electrodes. Furthermore, μcoils offer advantages such as MRI compatibility [24], spatial specificity, and directionality [25]. This technology was first reported over a decade ago in tests of solenoidal μcoils on rabbit retinal neurons *in vitro* [26]. Various μcoil shapes have been investigated in several different experimental settings. The optimized shape of the coil for neuromodulation is still under investigation, with several designs reported based on both computational modeling and experimental approaches [25–30]. Some of the notable experimental settings these μcoils have been tested in include *in vivo* intracortical μMS using V-shaped μcoils [28], *in vitro* focal control of pyramidal neurons with solenoidal μcoils [31], *in vitro* somatic and axonal inhibition of action potentials of ganglion cells in marine mollusk using solenoidal μcoils [32, 33], and *in vitro* activation of the CA3-CA1 synaptic pathway in hippocampal tissue slices [25].

Kagan *et al* [34] reported *in vivo* magnetic stimulation of the sciatic nerve using centimeter- and millimeter-scale solenoidal coils. Their work did not use μcoils and lacked additional experiments to prove that the stimulation effect on the rat sciatic nerve was indeed an effect of magnetic stimulation. In this work, we present μMS using the Magnetic Pen (MagPen) [25] on the rat sciatic nerve and report a dose-response relationship for μMS that confirms a micromagnetic stimulatory effect on the nerve. Based on MagPen's contact with the nerve, it offers extraneural activation. The spatial specificity that the MagPen offers is a function of the relative orientation of the μcoil to the tissue (see section 3.1), the angular contact of the MagPen with the nerve (see section 3.2), and the direction of the sinusoidal current through the μcoil. The depth of neural activation that the MagPen offers is a function of the magnitude of the induced electric field generated by the μcoil for a particular combination of amplitude and frequency of sinusoidal current (see section 3.5). In addition, the depth of activation also depends on how fast the induced electric field decays with distance between the μcoil and the nerve (see supplementary information S2). Therefore, peripheral nerve activation by the MagPen is unique, as it is attached to the nerve like a Cuff electrode but offers both extraneural and intraneural activation, similar to TIME. Furthermore, the ability to simply position the MagPen over the nerve makes this method significantly more versatile, as it does not need specialized surgical training for electrode penetration inside the nerve, as is the case for TIME, LIFE, and USEA. In their work on the micromagnetic activation of hippocampal tissue slices, Saha *et al* [25] briefly reported based on numerical simulations that the nature of micromagnetic activation is frequency dependent. Meaning, that at

higher frequency of the current driving the μcoils, the amplitude of the current through the μcoils required to activate the neural tissues is less; at lower frequency, a current of higher amplitude driving the μcoils is required to trigger neural activity. Although the report of such frequency-dependent activation of the neural tissues by μMS follows directly from Faraday's laws of electromagnetic induction, an experimental justification was missing. Herein, we measure the dose-response relationship of micromagnetic stimuli (varying amplitudes and durations) on hind limb twitches evoked via rat sciatic nerve activation. The results of this dose-response measurements of μMS experimentally confirm that the stimulatory effect of these μcoils is micromagnetic in nature rather than thermal or electrical [35]. Finite element analysis (FEA) has been previously used to study the thermal effects of Utah microelectrode arrays on grey matter tissues [36]. An experimental method to determine the temperature increase caused by Utah Arrays using infrared cameras in *in vitro* salt baths has also been previously reported [37, 38]. We have used FEA and numerical techniques to corroborate those *in vitro* salt bath temperature measurements to affirm that the nature of stimulation imposed by the MagPen is indeed micromagnetic. Overall, this work demonstrates the efficacy and feasibility of focal neuromodulation using μMS, which may open a new avenue for the study of *sciatica* and chronic pain management.

2. Materials and methods

2.1. MagPen: micromagnetic neurostimulation probe fabrication

The fabrication method of the micromagnetic neurostimulation probe, MagPen (see figure 1(a)), both Type Horizontal (Type H) and Type Vertical (Type V), has been reported previously [25]. In this work, we used a commercially available solenoidal μcoil (Model no.: TDK Corporation MLG1005SR10JTD25). Regarding the appropriate choice of the μcoil model, it was made sure that the electrical characteristics of the μcoil were reduced to that of a simple resistive–inductive (RL) circuit (see table S1 for LCR meter measurements of the RLC characteristics). Each μcoil was soldered (using solder flux & hot air blower) at the tip of a printed circuit board (PCB) with a length of 3 cm. For ease of orientation of the MagPen over the nerve, we thinned the PCB down to 0.4 mm along the z axis (see figure 1(a)). The tip of the MagPen where the μcoil is located has a width of 1.7 mm in Type H and 1.4 mm in Type V. A complete image of the prototype is provided in figure S1 of supplementary information S1. The μcoil measures 1 mm $\times$ 600 μm $\times$ 500 μm, which is smaller than the size of a pencil tip (Dixon No.2 HB pencil) (see figure 1(b)).

In the study of the neural activation capability of a micromagnetic implant, complete blockage of current leakage and capacitive current from the prototype is extremely essential. This requirement can be achieved by encapsulating the μcoil within a biocompatible polymer coating. In this study, we introduced a 10 μm-thick Parylene-C coating on the tip of the MagPen using a SCS-Labcoater Parylene-C deposition system. The efficacy of the current anti-leakage coating in the MagPen prototypes was validated by measuring the impedance between one terminal of the MagPen and laboratory-made standard artificial cerebrospinal fluid (aCSF) with a composition (in mM) of 124 NaCl, 2 KCl, 2 $MgSO_4$, 1.25 NaH_2PO_4, 2 $CaCl_2$, 26 $NaHCO_3$, and 10 D-glucose [39]. During the measurement of this impedance, the MagPen was immersed in the solution, and a single-cycle sinusoidal current of 2 A was driven at a frequency of 2 kHz with 1 s intervals. If the measured impedance was 5 MΩ and above, the prototype passed our quality control test. As further discussed in supplementary information S2, limiting the thickness of this Parylene-C coating is also essential, as the induced electric field drops rapidly with distance.

2.2. Circuit characteristics of the μcoil

An LCR meter (Model no. BK Precision 889B; see table S1 in supplementary information S1) was used to measure the resistance (R), inductance (L), and capacitance (C) values of the μcoil implant. The μcoil reduced to a RL series circuit. As per Faraday's laws of electromagnetic induction, the electromotive force (emf) is directly proportional to the series inductance (L_s). The relationship is given by the expression $v(t) = L_s \frac{di(t)}{dt}$, where $v(t)$ is the emf induced in an electrical circuit (here, neurons: the biological circuits) due to a time (t)-varying magnetic field ($B(t)$); $v(t)$ contributes directly to the induced electric field that will stimulate the neurons, and $\frac{di(t)}{dt}$ is the time derivative of the current through the μcoil ($i(t)$). The DC resistance (R_{DC}) of the μcoil contributes solely to the Joule heating of the μcoils during neuron activation [24, 40, 41] ($heat = i(t)^2 R_{DC} t$). A previous study by Minusa *et al* [27] reported a temperature increase of $\sim$1–1.5 °C in aCSF when the μcoils were driven by the alternating current necessary for neural activation. Recently, Jeong *et al* [38] used an optical probe to measure the temperature increase in the neural tissue during micromagnetic activation and reported a similar observation. Park *et al* [41] used FEA techniques to optimize the geometrical parameters of a planar μcoil such that the temperature rise in neural tissues is below 1 °C. We have performed an independent study involving experimental and numerical calculations of the heat energy released from the μcoil. The temperature change that is expected to be observed in the nerve from MagPen stimulation corroborates that of other reports

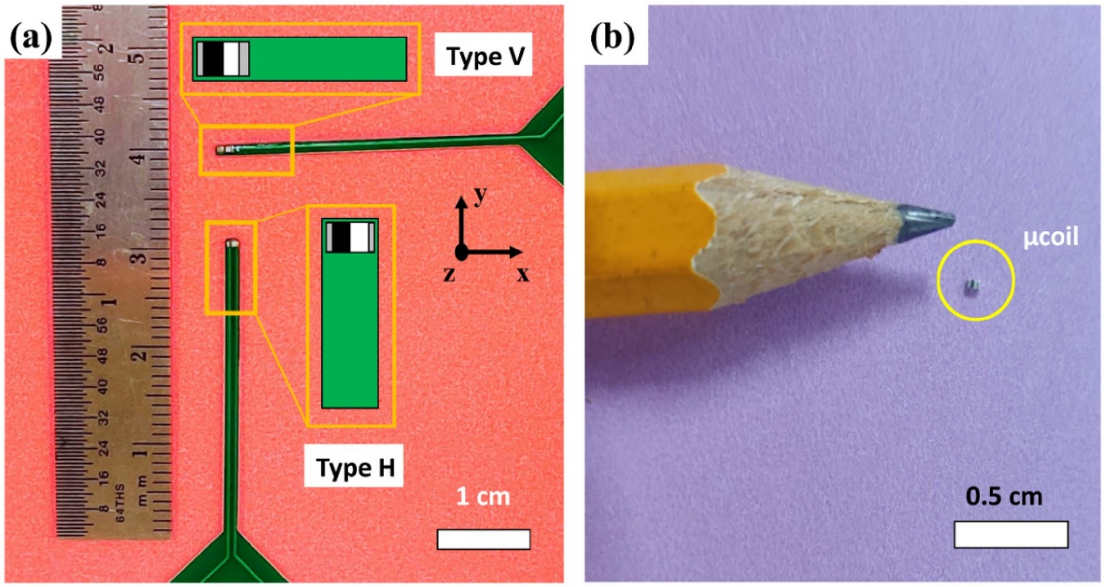

Figure 1. (a) The Magnetic Pen (MagPen) prototype fabricated in two different orientations: Type Horizontal, or Type H, and Type Vertical, or Type V. The implant, or the magnetic microcoil (μcoil), is situated at the tip. (b) Size comparison of the μcoil to the tip of a pencil (Dixon No. 2 HB pencil).

(see supplementary information S7). Overall, compared to the μcoil model used in our previous work ($R_{DC} = 3.8$–$4.4\ \Omega$) [25], the R_{DC} values for this μcoil are lower (between 1.8 Ω and 2.2 Ω), and we expect the heating effect to be two orders of magnitude lower.

2.3. Animal handling & surgery

All *in vivo* experiments were performed in accordance with a University of Minnesota-approved Institutional Animal Care and Use Committee protocol. Seven 349 ± 91 gram Long–Evans rats were administered 1200 mg kg^{-1} Urethane anesthesia through intraperitoneal injection and given 4 mg kg^{-1} Lidocaine and 2 mg kg^{-1} Bupivacaine local anesthesia via subcutaneous injection at the incision site [42]. Urethane was used to preserve the neurochemical environment of the rat. The rat was placed on an appropriate heating device, and supplemental oxygen was given via nose cone throughout the experiment. A 30 mm incision exposed the dorsal-medial right quadricep muscular interstitial space where the sciatic nerve could be accessed. One cotton-tipped applicator was placed between the sciatic nerve and the quadricep for effective placement of the μcoil (see figure 2(a)(i)). Anesthetic depth and vital signs were monitored every 15 min throughout the experiment to ensure rat comfort and homeostasis.

2.4. The 'Dose': MagPen driving circuitry

The MagPen driving circuitry and the associated waveforms are illustrated in figure 2(b). The stimulus was applied to the sciatic nerve using a function generator (Model no. RIGOL DG1022Z) as single-cycle sinusoids with 1 s intervals (see Waveform in figure 3). The current through the μcoil ($i(t)$) is represented by the equation $i(t) = A_1 \sin 2\pi ft$, where A_1 and f are the current strength/amplitude and frequency through the μcoil, respectively. The $1/f$ component is equivalent to the duration of the micromagnetic stimulus. A_1 and f consist of a significant component of the 'dose'. The current, $i(t)$, is amplified by a class-D amplifier (Model no. Pyramid PB717X) set at a constant gain, A. An alternating current drives the μcoil to generate a time-varying magnetic field ($B(t)$). As per Faraday's law of electromagnetic induction, this time-varying magnetic field induces an electric field (E_{ind}), which activates the nerve. The field is expressed by the equation $\oint \boldsymbol{E}_{\mathbf{ind}} \cdot \mathrm{d}\boldsymbol{l} = -\iint \frac{\partial \boldsymbol{B}(t)}{\partial t} \cdot \mathrm{d}\boldsymbol{S}$. Therefore, we obtain the expression $E_{ind} \propto \frac{\mathrm{d}B(t)}{\mathrm{d}t} \propto \frac{\mathrm{d}i(t)}{\mathrm{d}t}$. Hence, on applying a sinusoidal current waveform ($i(t)$) through the μcoil, we will obtain an induced electric field waveform (E_{ind}) in the form of a time-derivate of the current. As this induced electric field activates the nerve, it induces a sinusoidal current ($J(t)$) in the nerve, which activates the axons in it (see figure 2(b)).

2.5. Finite element modeling (FEM) of the μcoil

It is challenging to experimentally measure the magnetic field and the corresponding induced electric field from these sub-mm-sized μcoils. Minusa *et al* [27] reported the use of miniaturized, custom-made pick-up coils for this purpose. For such measurements, it is extremely essential to place the μcoil implants close to the pick-up coils. Khalifa *et al* [43] reported the use of nitrogen vacancy magnetometers to measure the induced electric field from these μcoils. A cost-effective yet reliable way

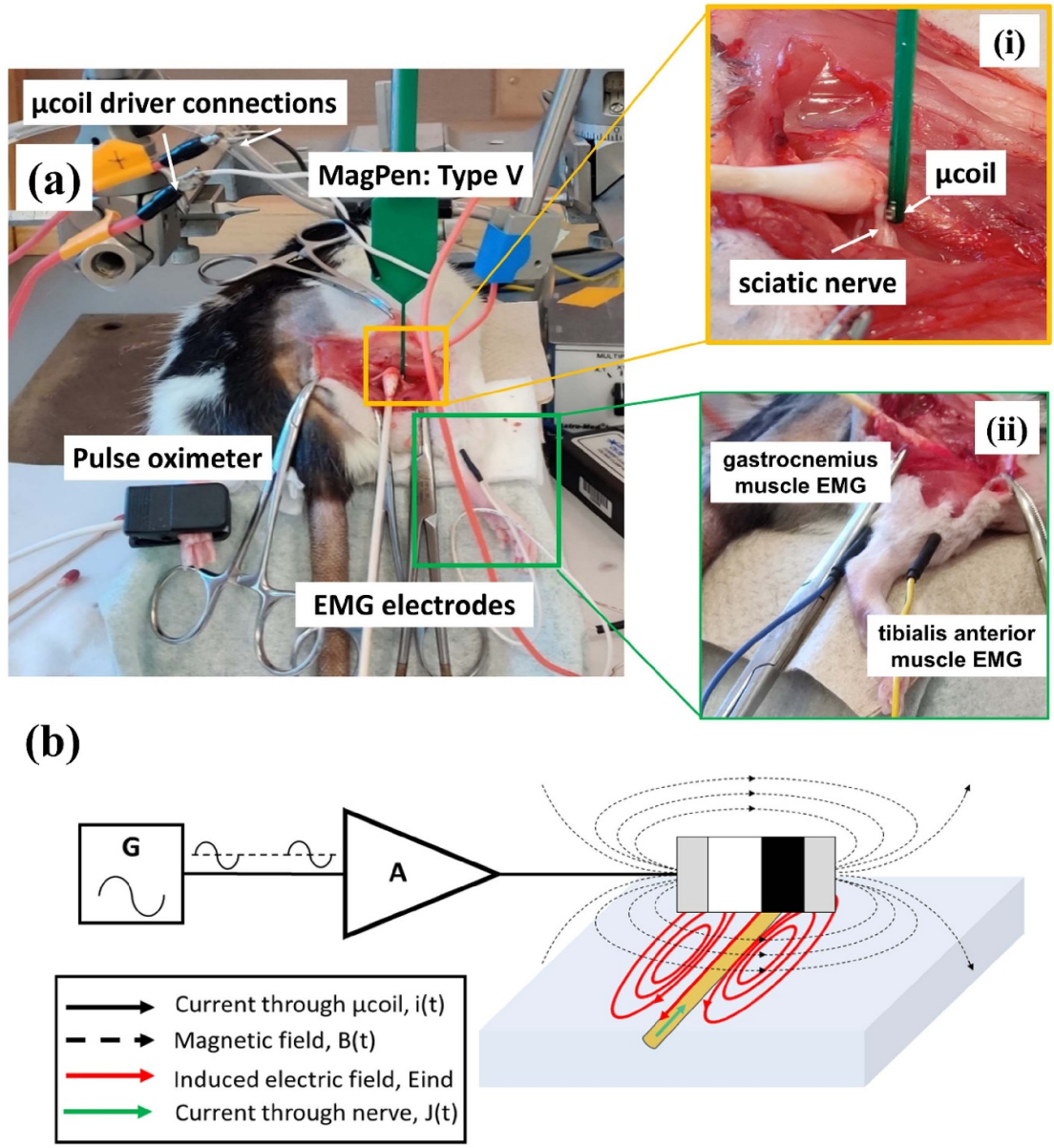

Figure 2. Experimental set-up for studying the effect of μMS on the rat sciatic nerve. (a) The right sciatic nerve of a rat under anesthesia has been surgically exposed, and the MagPen: Type V has been placed over the nerve. A pulse oximeter continually measures the heart rate and oxygen saturation in the blood of the rat. The power source connections driving the μcoil have been marked. (i) A more detailed orientation of the μcoil (MagPen: Type V) on the rat sciatic nerve that activated the nerve fibers. (ii) EMG electrodes have been inserted in the front and back muscles of right hind limb of the rat. (b) The MagPen driving circuit consists of a function generator (G), which generates single-cycle bursts of sinusoidal waveforms of varying amplitude and duration. This waveform is amplified by a class-D amplifier set at a constant 10× gain, thereby generating the current that drives the μcoil (denoted by solid black lines). This amplified current, when fed into the μcoil, generates a time-varying magnetic field (denoted by dotted black lines), which in turn induces an electric field (denoted by solid red lines) on the nerve. This induced electric field generates a current through the nerve (denoted by solid green lines).

to conduct such magnetic field and induced electric field measurements is the numerical modeling of electrical currents in neural tissues using FEM-based calculations [44–46]. In this work, we used the eddy current solver of ANSYS-Maxwell [47] (ANSYS, Canonsburg, PA, United States) to study the magnetic field and the induced electric field from the μcoils. It solves an advanced form of the T–Ω formulation of Maxwell's equations [48]. The μcoil ceramic core dimensions, tissue slab parameters, boundary conditions, and high-resolution tetrahedral mesh size used in the model are detailed in table 1. All the modeling work was performed using the Minnesota Supercomputing Institute at the University of Minnesota (8 cores of Intel Haswell E5-2680v3 CPU, $64 \times 8 = 512$ GB RAM and 1 Nvidia Tesla K20 GPU). The induced electric field values were then exported for analysis using a customized code written in MATLAB (The Mathworks, Inc., Natick, MA, USA). For the numerically simulated spatial contour plots of the magnetic field ($B_{x,y,z}$) and induced electric field ($E_{x,y,z}$), refer to supplementary information S6.

Table 1. FEM modeling parameters for the μcoil.

Parameter description	Value
μcoil dimensions (L × W × H)	1 mm × 600 μm × 500 μm
Number of turns (N)	21
Wire diameter	7 μm
Tissue dimension (L × W × H)	4 mm × 4 mm × 300 μm
Conductivity of tissue (σ)	0.13 S m^{-1}
Air dimension (L × W × H)	10 mm × 10 mm × 4 mm
Energy error (user-specified)	1%
Final solution no. of mesh elements	410 000
Adaptive passes (converged)	6

The magnetic and electric fields induced by μcoils are highly directional, and so the sensitivity of nerves to μMS will be highly orientation-dependent [25, 49]. In our previous work [25] using the MagPen for the *in vitro* activation of the hippocampal CA3-CA1 synaptic pathway, we had generated induced electric field spatial profiles from ANSYS-Maxwell for both MagPen: Type H and MagPen: Type V. Performing NEURON simulations (https://neuron.yale.edu/neuron/) on the induced electric field spatial profiles, we reported that when the MagPen's long axis was oriented out-of-plane with respect to the tissue, the simulated pyramidal neuron was activated. When the MagPen's long axis was oriented in-plane with respect to the tissue, the neuron at the same location as in the previous case could not be activated [25]. Further investigation into the orientation-dependent activation of the μcoils in this work helped us to conclude that the orientation of the neurons in the tissue with respect to the long axis of the μcoil also plays a key role in successful activation (see figure 4).

2.6. The 'Response': recording and tracking the hind limb movement activity

Stimulation of the rat sciatic nerve activates the hind limb, causing the leg muscles to twitch. To record limb muscle activation, we used EMG electrodes (Model no. Disp. Subdermal Needle-27 ga. 12 mm from Rochester Electro-Medical Inc.) in the tibialis anterior and gastrocnemius leg muscles of the rat (see figures 2(a)(ii) and 3(c)). EMG electrodes were connected to a headstage (Intan 32ChRHD2132), and muscle activity was recorded at 30 kHz with an Open-ePhys system (https://open-ephys.org/). EMG recordings are shown in figure S3 in supplementary information S3.

Due to the close proximity of the MagPen and the EMG electrodes, there were significant stimulus artifacts in the EMG signals. In addition to the EMG recording, we also measured the leg twitch activity via video tracking for image processing. A WebCam (LogiTech C270 WebCam; 720p & 30 fps) was used to record the hind limb movements. To aide subsequent image processing, a patch of green tape was attached to the foot. Video was collected (see supplementary video SV1) while stimulating the sciatic nerve with the MagPen at 1 Hz. The image data were processed using MATLAB's Computer Vision ToolBox (The Mathworks, Inc., Natick, MA, USA) and a customized code for motion tracking developed using MATLAB (see figure 3(d)). For data analysis, images were cropped around the green tape placed on the limb (see supplementary video SV2). A total of 9 s of data were analyzed. Movement was calculated by tracking changes in the green tape in the video. A Kalman filter was used to remove noise in the resulting signal. The pixel changes were tracked and predicted inside boundary boxes (bboxes) (see supplementary information S4: Pictorial demonstration of the Image Processing Algorithm).

3. Results

3.1. Orientation specificity of the μcoil with respect to the nerve

In our experimental set-up in figure 2(a), both MagPen prototypes, Type H and Type V, were tested on the sciatic nerve. Only MagPen: Type V helped us achieve the orientation for successful hind limb movement (see figure 2(a)(i)). In this section, we provide physics-based justifications for the orientation specificity of μMS. In figure 4, we schematically represent how various orientations of the μcoil relative to the tissue and the corresponding arrangement of nerve fibers (yellow cylinders in figure 4) affect the directionality of the induced electric field. This also affects how a nerve is activated by μMS.

Figure 4(a) shows how bipolar electrical stimulation electrodes activate the nerve. Nerves are activated due to membrane hyperpolarization and membrane depolarization from the electrode tips. For a μcoil, when the long axis is oriented in-plane with the tissue (MagPen: Type H) and the nerve is aligned along the x axis (see figure 4(b)), due to the directionality of the induced electric fields (shown as solid red lines), it successfully activates the nerve. For the same μcoil orientation but with the nerve fiber aligned along the y axis (see figure 4(c)), the directionality of the induced electric field from the μcoils does not favor successful membrane hyperpolarization and

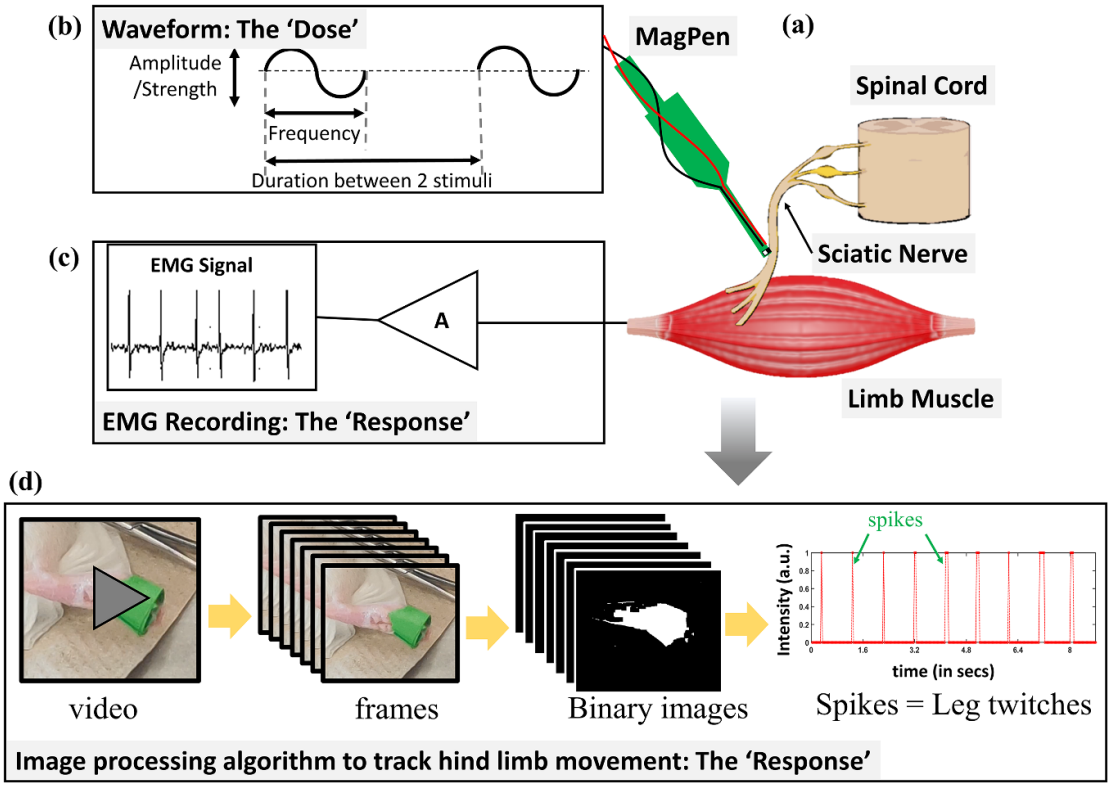

Figure 3. Schematic overview of the *in vivo* MagPen-sciatic nerve experimental set-up. (a) The sciatic nerve originates from the spinal cord and projects to the hind limb muscles. In this work, we used MagPen: Type V (single μcoil prototype) to demonstrate micromagnetic activation of the sciatic nerve. (b) The 'Dose': The MagPen was driven by a single wave of a sinusoidal current waveform of varying amplitude and frequency; each stimulus is separated by 1 s. (c) The 'Response': stimulation of the sciatic nerve evoked electrical activity in the muscle, which was recorded using electromyography (EMG) in the limb muscles. (d) In addition, hind limb movement was tracked by applying an image processing algorithm to the video recording of the hind limb movement obtained from μMS.

depolarization. For similar reasons, in figure 4(d), when the long axis of the μcoil is out-of-plane with respect to the tissue (MagPen: Type V) and the nerve is aligned along the x axis, it cannot be activated. However, by keeping the same orientation of the μcoil relative to the tissue as that shown in figure 4(d) (MagPen: Type V) but aligning the nerve along the y axis (see figure 4(e)), the nerve can be activated. Our findings closely corroborate those of Golestanirad *et al* [49].

In this *in vivo* experiment, we tried to position the μcoil with respect to the nerve fibers as shown in figure 4(b) (Type H) or in figure 4(e) (Type: V). However, only the orientation in figure 4(e) (Type V) successfully activated the sciatic nerve and showed hind limb movements. We believe that for the orientation shown in figure 4(b) for Type H, the nerve fascicles that were responsible for hind limb movements were not activated due to the spatially specific nature of μMS. It might also be possible that the induced electric field magnitude was not sufficient to activate the nerve fascicles (see figure 5(a)(iii)). However, for the orientation in figure 4(e) for Type V, those specific fibers in the sciatic nerve were successfully activated. This is where the orientation specificity of the μcoils is significant in this work. In section 3.2, we have further quantified the angular dependence of the μcoils with respect to the neural tissue on the magnitude of the induced electric field.

3.2. Angular significance of the μcoil with respect to the neural tissue

Our previous report already showed that the MagPen offers spatially specific activation of the neural tissues [25]. The μcoil in the MagPen can activate a maximum of 2.672 mm^2 (out of 16 mm^2) of the tissue area (see the black dotted line in figure 5(e)(iii)) [25]. However, in previous studies, the angular orientation of the μcoil with respect to the tissue and its contribution to spatially specific activation has not been investigated in detail. While trying to place the MagPen over the sciatic nerve at reproducible locations, as in figures 4(b) or (e), there were several experimental instances (estimated to be caused by motion of the hind limb upon successful activation or breathing of the rat, etc) where the angular orientation of μcoil to the nerve changed. This resulted in a change in the stimulation threshold, as measured by activation of the hind limb. Figure 5 shows a simulation of the spatial contour map of the induced

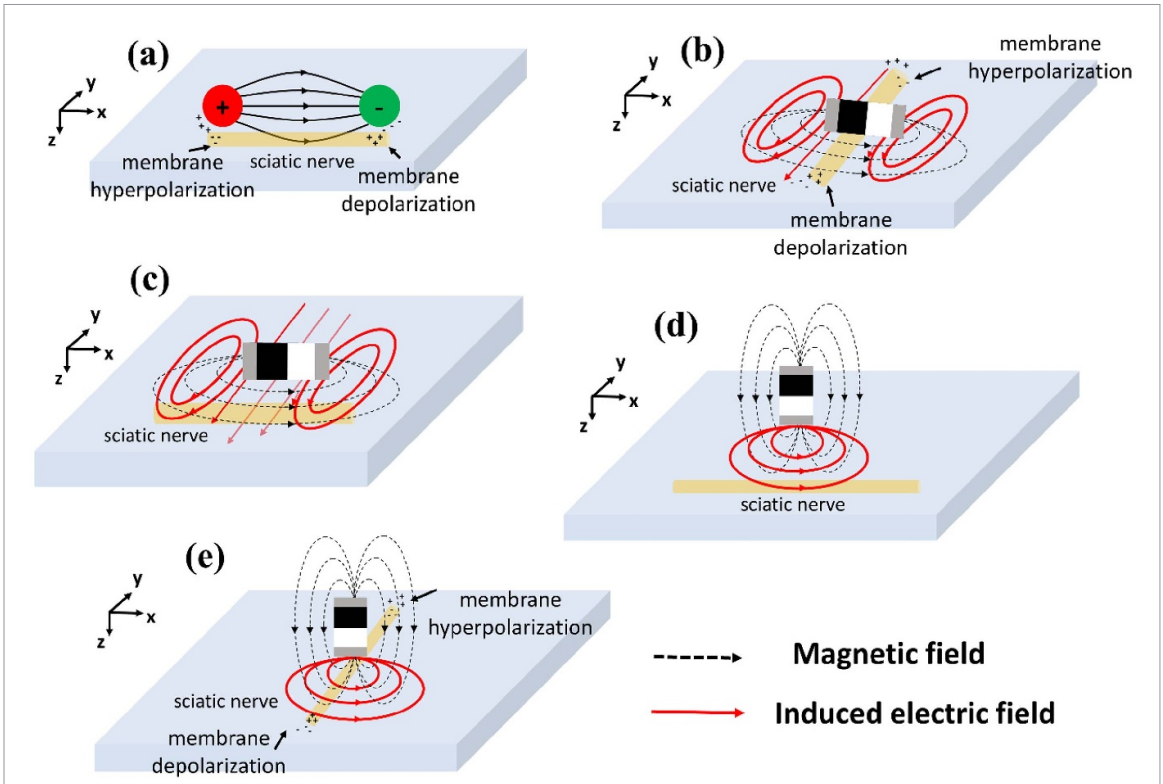

Figure 4. Schematic representation of the importance of the directionality/orientation of the μcoil with respect to the nerve for successful activation of the nerve using μMS. (a) Mechanism of activation of the sciatic nerve using bipolar electrical electrodes. (b) Long axis of the μcoil in-plane to the tissue (MagPen: Type H) and nerve aligned along the *y* axis. (c) Long axis of the μcoil in-plane to the tissue (MagPen: Type H) and nerve aligned along the *x* axis. (d) Long axis of the μcoil out-of-plane to the tissue (MagPen: Type V) and nerve aligned along the *x* axis. (e) Long axis of the μcoil out-of-plane to the tissue (MagPen: Type V) and nerve aligned along the *y* axis.

electric field as the μcoil changes angular orientation relative to the nerve. The spatial contour plots of the induced electric field demonstrate that in addition to the magnitude of current driving the μcoils, the angular orientation of the μcoils relative to the tissue also alters the magnitude of the induced electric field (see figures 5(a)(iii), (b)(iii), (c)(iii), (d)(iii) and (e)(iii)). Furthermore, whether the angular orientation of the μcoil activates the nerve depends on the alignment of the nerve (see figure 4). This fact affected our experiments while studying MagPen's efficacy in activating the sciatic nerve. The neural activation probability was lowest for the angular orientations in figure 5(a)(i) (achieved by MagPen: Type H) and figure 5(e)(i) (achieved by MagPen: Type V). The greatest probability of neural activation was for the angular orientations in figure 5(a)(ii) (achieved by MagPen: Type H) and figure 5(e)(ii) (achieved by MagPen: Type V). Tedious efforts were made to ensure that the orientation of the MagPen on the sciatic nerve was as shown in figure 5(a)(ii) (achieved by MagPen: Type H) and/or figure 5(e)(ii) (achieved by MagPen: Type V). This is the same condition as shown in figures 4(b) and (e), respectively. If, due to human error, the MagPen was oriented under any of the other conditions shown in figure 5, a much higher magnitude of current would be required to trigger hind limb movements. However, in figures 5(a)(i) and (e)(i), which are the same conditions as those shown in figures 4(c) and (d), no hind limb movement was observed. However, in the experiments, only MagPen: Type V (see figures 2(a)(i) and 5(e)(ii) showed successful hind limb movements because the induced electric field magnitudes were greater compared to those generated by MagPen: Type H (see figures 5(a)(iii) and (e)(iii)).

Summarizing figure 5, a particular orientation of the μcoil with respect to the tissue generates a specific induced electric field contour plot. Whether that induced electric field spatial distribution activates the nerve depends entirely on the alignment of the nerve relative to the μcoil. This is the reason why only the condition in figure 5(e)(ii) (MagPen: Type V) activates the nerve despite figures 5(e)(i) and (e)(ii) having the same induced electric field spatial distributions. Supplementary information S9 has further quantified the effect of the angular orientation of the μcoil on the induced electric field.

3.3. Frequency dependence of the induced electric field

Our previous work with the MagPen to activate the CA3-CA1 synaptic pathway in hippocampal slices [25] also reported a numerically simulated 'strength-frequency' plot of μMS. When the μcoils are driven

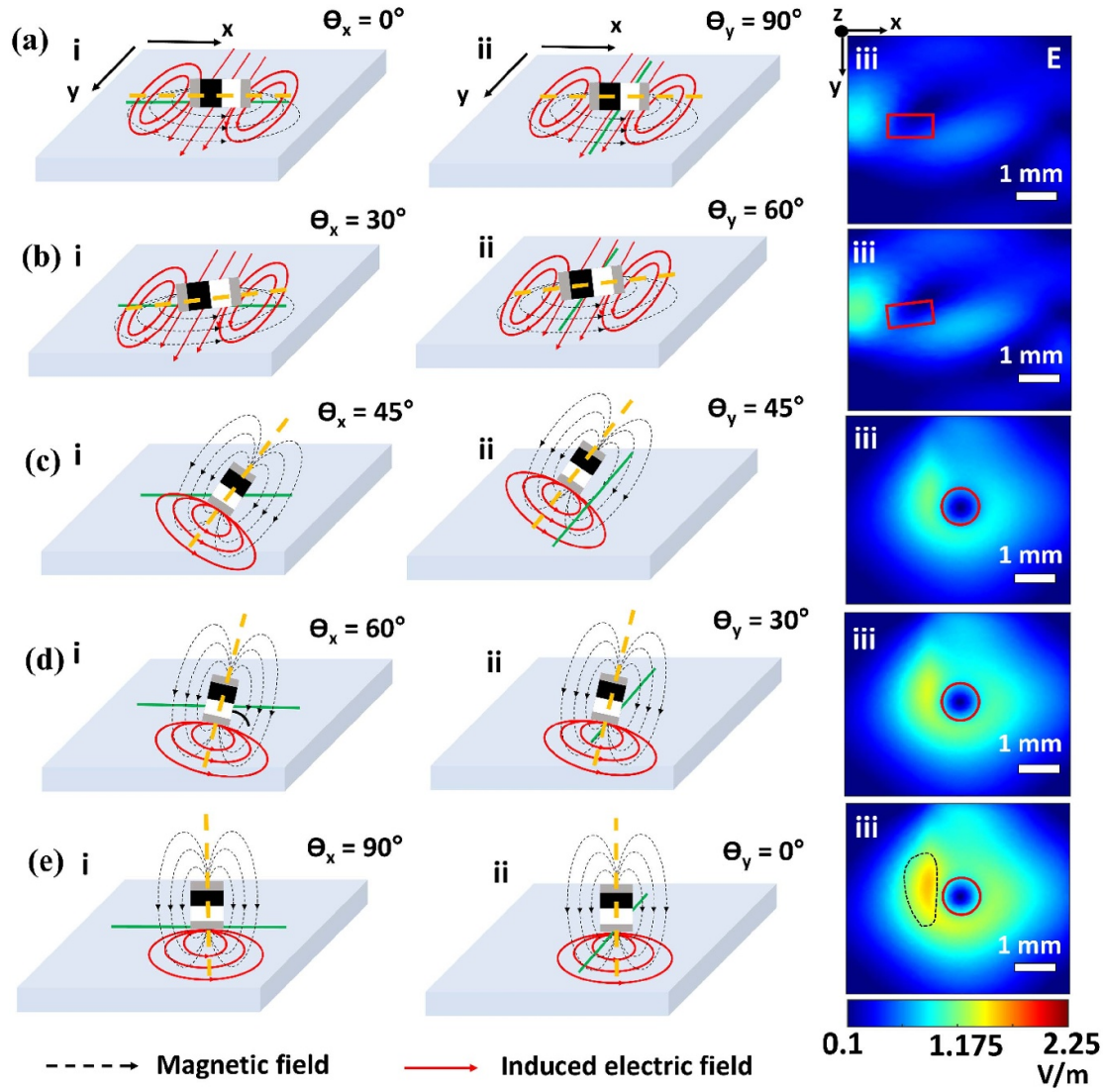

Figure 5. Schematic demonstration of the angular dependence of the μcoil with respect to the nerve alignment along both the x and y axes in the plane of the nerve tissue. The long axis of the μcoil is represented by a dashed yellow line. The alignment of the nerve fiber in the tissue is represented by a solid green line. The red outline denotes the location of the bottom side of the μcoil with respect to the tissue. (a)(i) $\theta_x = 0°$ (same as figure 4(c)), (ii) $\theta_y = 90°$ (same as figure 4(b)), (iii) normalized induced electric field on a tissue projected along z direction. (b)(i) $\theta_x = 30°$, (ii) $\theta_y = 60°$, (iii) normalized induced electric field on a tissue projected along z direction. (c)(i) $\theta_x = 45°$, (ii) $\theta_y = 45°$, (iii) normalized induced electric field on a tissue projected along z direction. (d)(i) $\theta_x = 60°$, (ii) $\theta_y = 30°$, (iii) normalized induced electric field on a tissue projected along z direction. (e)(i) $\theta_x = 90°$ (same as figure 4(d)), (ii) $\theta_y = 0°$, (same as figure 4(e)) (iii) normalized induced electric field on a tissue projected along z direction. The black dotted outline denotes 2.672 mm^2 (out of 16 mm^2) of the tissue area that has the maximum probability of getting activated. ($\theta_x + \theta_y = 90°$). The distance between the μcoil and neural tissue is taken to be 100 μm along the z axis. The μcoil was driven by a sinusoidal current of 2 A at a frequency of 2 kHz.

by a time (t)-varying single-cycle sinusoidal current of frequency f and amplitude A_1, the current (in units of ampere (A)) through the μcoil can be expressed as:

$$i(t) = A_1 \sin 2\pi f t. \tag{1}$$

This amplitude, A_1, of the current through the μcoil can also be written as:

$$A_1 = \frac{V}{R} \tag{2}$$

where V is the voltage applied to the μcoil (in volt (V)) from the driving circuit, as in figure 2(b), and R is the resistance of the μcoil (in ohm (Ω)). This current $i(t)$ generates a time-varying magnetic field $B(t)$ given by the equation:

$$B(t) = \frac{\mu_r \mu_0 i(t) N}{L} \tag{3}$$

where, μ_r is the relative magnetic permeability of the medium, μ_0 is the vacuum permeability, N is the number of turns in the μcoil, and L is the length of the μcoil. This magnetic field, as per Faraday's laws of electromagnetic induction, induces an electric field ($\boldsymbol{E}_{\mathbf{ind}}$) in the medium that is expressed by the following equation:

$$\oint \boldsymbol{E}_{\mathbf{ind}} \cdot \mathrm{d}\boldsymbol{l} = -\iint \frac{\partial \boldsymbol{B}(\boldsymbol{t})}{\partial t} \cdot \mathrm{d}\boldsymbol{S} \tag{4}$$

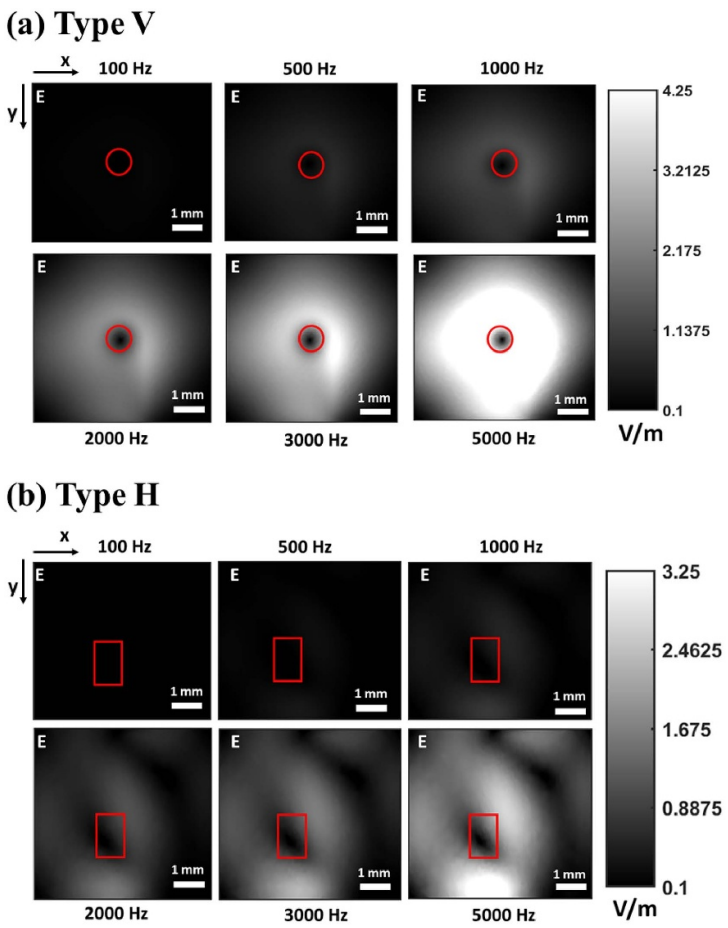

Figure 6. FEM modeling showing that with an increase in the frequency of the sinusoidal stimulus, there is an increase in the induced electric field magnitude. The working window shows the numerically simulated normalized induced electric field (E in V m^{-1}) calculated for a μcoil being driven by a current of 2 A at varying frequencies. The E was measured on a tissue of dimensions 4 mm $\times$ 4 mm $\times$ 300 μm. The distance between the μcoil and neural tissue is taken to be 100 μm. Frequency dependence of the induced electric field for (a) MagPen Type V (b) MagPen Type H. The position of the μcoil with respect to the tissue has been marked with a solid red boundary.

where, $\boldsymbol{l}$ and $\boldsymbol{S}$ are the contour and the surface area of the neural tissue, respectively. By substituting the expressions for $\boldsymbol{B}(\boldsymbol{t})$ and $\boldsymbol{i}(\boldsymbol{t})$ in equation (4) followed by some basic differentiation, we obtain the value of $\boldsymbol{E_{ind}}$ as follows:

$$\oint \boldsymbol{E_{ind}} \cdot \mathrm{d}\boldsymbol{l} = -\frac{\mu_r \mu_0 N}{L} . A_1 . f . 2\pi . \cos(2\pi f t) \iint \mathrm{d}\boldsymbol{S} \tag{5}$$

$$\oint \boldsymbol{E_{ind}} \cdot \mathrm{d}\boldsymbol{l} = -\frac{\mu_r \mu_0 N}{L} \cdot \frac{V}{R} . f . 2\pi . \cos(2\pi f t) \iint \mathrm{d}\boldsymbol{S}. \tag{6}$$

From equation (5), we deduce that $E_{\mathrm{ind}} \propto A_1 . f$, indicating that the value of the induced electric field is directly proportional to the two significant components of the 'dose': the amplitude (A_1) and the frequency (f) of the sinusoidal current driving the μcoil (see section 2.4). Keeping all the other variables in equation (5) constant, to achieve a particular value of E_{ind} necessary for nerve activation, if either component of the 'dose' for μMS (A_1 or f) is increased, the other component can be decreased. This frequency dependence of the induced electric field is a unique feature of μMS that directly obeys Faraday's laws of electromagnetic induction. Figures 6(a) and (b) show that the magnitude of the induced electric field increases with frequency for both MagPen orientations (i.e. Type V and Type H) while the current driving the μcoils is kept constant. Equation (6) has been obtained from equation (5) by substituting equation (2) into equation (5). In this work showcasing μMS of the rat sciatic nerve, we have experimentally demonstrated this frequency-dependent phenomena (details explained in section 3.5). For numerically simulated spatial contour plots of the magnetic field ($B_{x,y,z}$) and induced electric field ($E_{x,y,z}$), refer to supplementary information S6.

3.4. Tracking hind limb movement using image processing algorithms

The successful activation of the sciatic nerve by MagPen stimulation has been determined from muscle twitches causing foot dorsiflexion. We recorded the dorsiflexion movements using videos. Figure 7(a)

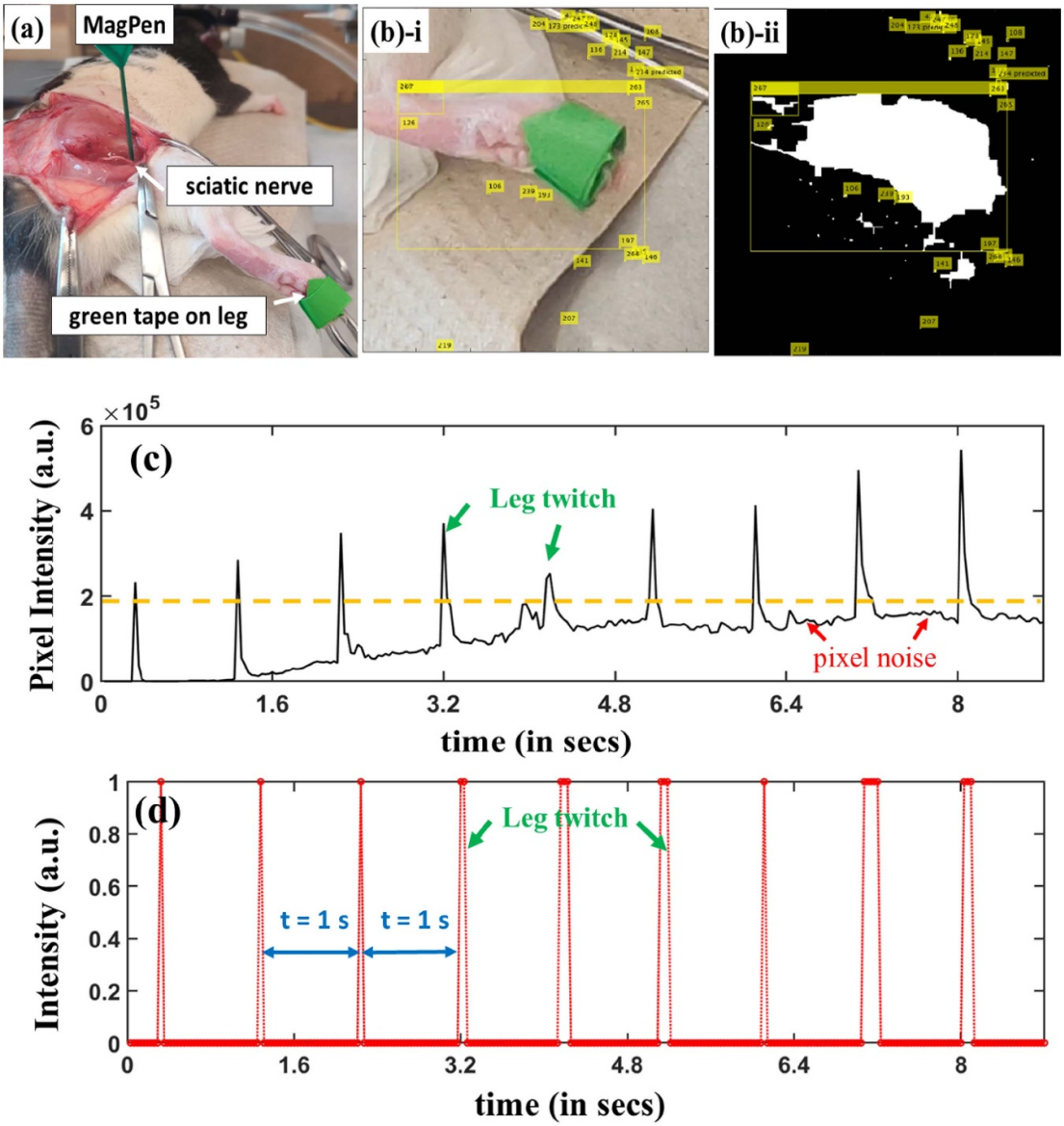

Figure 7. Image processing algorithm used to detect leg muscle twitches/movement from a 9 s-long video sampled at 30 Hz with the MagPen activating the sciatic nerve at 1 s intervals. (a) A rat under anesthesia with the right sciatic nerve surgically exposed and green tape attached to the leg. (b)(i). The algorithm classifies a bbox around the rat leg keeping the green tape on the leg as a centroid for the bbox. (b)(ii). The binary image formed from the image in (b)(i) color-codes the green tape on the leg as white pixels (see the area under the bbox). (c) Sum of the white pixels in each frame (pixel noise unfiltered). (d) Pixel noise filtered using a pixel intensity threshold (denoted by the dotted yellow line) from figure 7(c). This gives rise to distinct peaks separated by 1 s, where each peak corresponds to sciatic nerve activation by the MagPen. The 'dose' driving the MagPen was a single-cycle sinusoidal waveform of three $V_{p\text{-}p}$ amplitude at a frequency of 1 kHz; each cycle was separated by 1 s.

shows the experimental set-up in which green tape is wrapped around the toe of the right hind limb of the rat with the MagPen held over the sciatic nerve. Figure 7(b)(i) is a single frame from the 9 s video (see supplementary video SV2) showing the successful tracking of the green tape-wrapped hind limb inside the bbox (marked with a yellow outline in figures 7(b)(i) and (b)(ii)). Using the image processing algorithm explained in detail in section 2.6, we successfully created a binary image of the tracked limb, as shown in figure 7(b)(ii). The sum of 0s in the matrices defining each binarized frame is a measure of the white space in the frame. In figure 7(c), we plot the variation in the observed white space over the 275 frames of the 9 s video. In frames where limb movement was detected, a greater patch of white is observed, represented via the spikes observed in figure 7(c). The MagPen was driven by a single-cycle sinusoidal waveform of 3 $V_{p\text{-}p}$ amplitude at a frequency of 1 kHz, and stimulus was delivered at 1 s intervals. Therefore, following equations (1) and (2), $V = 3\,V_{p-p}$ and $f = 1\,\text{kHz}$. Since the micromagnetic stimulus was applied at 1 s intervals, we expect to observe a leg twitch every 1 s. To distinguish the spikes from the noise generated by the algorithm, a threshold is applied (the dotted yellow line in figure 7(c)). The result clearly shows nine distinct spikes at 1 s intervals, as shown in figure 7(d). Those

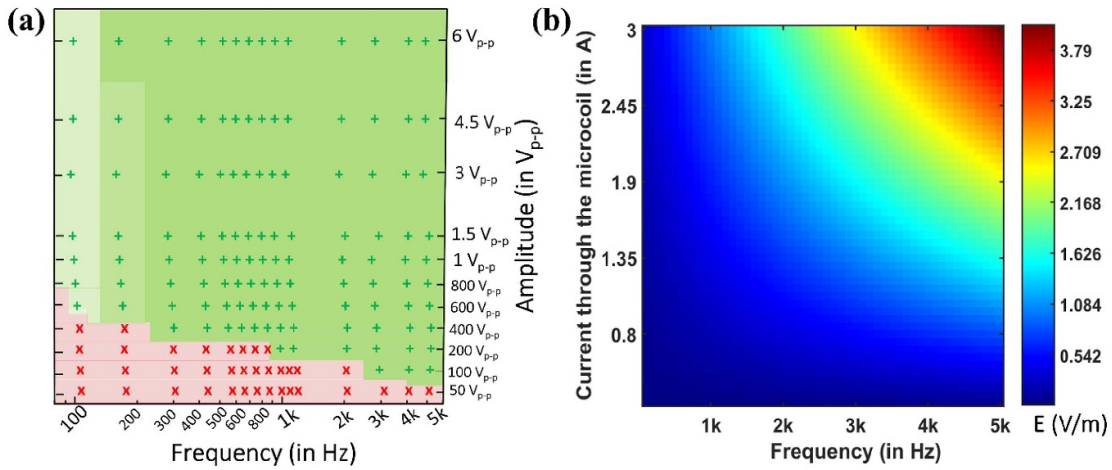

Figure 8. (a) The dose-response relationship experimentally measured by μMS of the rat sciatic nerve ($n = 7$). In this plot, the 'dose' is the amplitude (in $V_{p\text{-}p}$) and frequency (in Hz) of the μMS. The 'response' is the intensity of the rat hind limb muscle twitch observed. The green '+' symbols indicate the μMS that elicit hind limb movements in all seven rats independently. The red '*x*' symbols indicate those that did not elicit hind limb movements in any of the seven rats independently. Areas shaded in light, moderate and dark green represent parameters with weak, moderate, and strong leg responses, respectively. (b) Numerically simulated variation in the normalized induced electric field value (E in V m^{-1}) with the current through the μcoil (in A). The current through the μcoil (in A) = Amplitude (in $V_{p\text{-}p}$)/Resistance of the μcoil (in Ω).

nine spikes were observed throughout the MagPen stimulation period. In this way, we have successfully tracked hind limb movements following μMS of the rat sciatic nerve using image processing. EMG recordings were also used to monitor muscle activation (see supplementary information S3). However, due to the proximity of the MagPen to the EMG electrodes, large stimulus artifacts were observed. More image processing results are provided in supplementary information S5. We have applied image processing algorithms to supplementary video SV3 and showed that the algorithm can successfully track limb movements, identifying leg kicks at three-second intervals, corresponding to the μMS interval.

3.5. The dose-response relationship for μMS

We varied the 'dose' of the micromagnetic stimulus and measured the 'response', as determined by whether there was a measurable twitch in the hindlimb (see figure 8(a)). The twitch response was measured as we varied the stimulation peak-to-peak voltage ($V_{p\text{-}p}$) and the frequency of the single-cycle sinusoidal current (corresponding to the duration of the micromagnetic stimuli). We found four behaviors that were later used to classify the responses: (1) no leg movement; (2) weak leg movement; (3) moderately strong leg movement; and (4) strong leg movement. Here, 'leg movement' refers to the right hind limb movement of the rat. The dose-response relationship reported in figure 8(a) was measured for seven rats independently ($n = 7$).

Summarizing figure 8(a), we observe that for a dose with lower frequency (f) (higher duration of the micromagnetic stimulus ($1/f$)) and lower voltage ($V_{p\text{-}p}$), there is no leg movement (see supplementary video SV5). For lower frequency (f) (higher duration of the micromagnetic stimulus ($1/f$)) but high voltage ($V_{p\text{-}p}$), there is weak leg movement (see supplementary video SV4). At moderate frequency (f) and higher voltage ($V_{p\text{-}p}$), there is moderately strong leg movement (see supplementary video SV6). Finally, at high frequency (f) (lower duration of the micromagnetic stimulus ($1/f$)) and higher voltage ($V_{p\text{-}p}$), there is strong leg movement (see supplementary video SV2). The intensity of the hind limb movement is characterized in figure S3 (see supplementary information S3). This phenomenon and its frequency-dependent characteristic can be directly explained by Faraday's laws of electromagnetic induction, as explained in section 3.3 and figure 8(b). The amplitude of the response agrees well with the amplitude of the estimated induced electric fields (from equation (6)).

4. Discussion

This work is the first report of the micromagnetic activation of the rat sciatic nerve using sub-mm-sized μcoils. We observed a dose-response relationship for μMS that follows directly from Faraday's laws of electromagnetic induction [25]. The fact that we were able to observe this frequency-dependent phenomenon experimentally validates the hypothesis that we were activating the sciatic nerve using μMS rather than through electrical stimulation contributed by current leakage from the μcoils; in electrical stimulation, one would expect to observe strong leg movements at higher duration-higher amplitude combinations and weak leg movements at lower duration-higher amplitude combinations. Furthermore, this dose-response relationship further confirms that the frequency-dependent activation of the sciatic nerve cannot be the result of the Joule

heating effect from the μcoils [38] (see supplementary information S7). To prevent activation of the sciatic nerve through current leakage at the μcoil connections of the MagPen, a water-tight and biocompatible coating was used to insulate the MagPen. The thickness of the coating was less than 100 μm so as not to affect the induced electric field because the field strength decreases rapidly with distance (see supplementary information S2). The waveform driving the MagPen needs to be carefully determined, as it controls the Joule heating of the μcoils. Maintaining an appropriate time interval between two consecutive stimuli is key to properly dissipate the thermal energy that may cause the neural tissue to heat up (see supplementary information S7). In a study by Park and Kim [50], the thermal effects from planar-shaped micromagnetic coils were investigated using FEA. The major highlights of their work included optimizing the geometrical parameters of a planar coil and the stimulation parameters (pulse width, frequency, amplitude, and shape of the driving waveforms) such that the temperature rise in the neural tissues remained below 1 °C. However, all such optimizations were made while keeping the desired induced electric field constant at 10 V m^{-1} to ensure activation of the neural tissues. Keeping the induced electric field constant while optimizing the geometrical parameters of the coil and stimulation parameters is potentially a great fallacy of their work, as the induced electric field is frequency-dependent (or dependent on the stimulation parameters) [25]. Furthermore, the study lacks a comparison of the thermal effects of different shapes of the coils (such as solenoid, planar rectangular helix, or planar circular helix), which could contribute to future work in this field of study.

As expected from the induced electric field directionality, the orientation of the μcoil relative to the neural tissue strongly modulates the response (see section 3.1). However, in this work, we showed that the alignment of the nerve with respect to the μcoil in the tissue is also critical. For induced electric fields with the same spatial contours, the direction along which the nerve is aligned determines whether the μcoil will ultimately activate it. This unique feature of μMS highlights both strength of the neuromodulation technique and one of its fatal flaws. The orientation dependence of activation contributes to the directionally sensitive and spatially specific activation of the nerve. However, after long-term implantation of the μcoil within the human body to activate a peripheral nerve, implant movement due to unavoidable circumstances might alter the μcoil's contact with the nerve [51]. We hereby propose the design of a MagPen-Hook prototype where a hook will hold the nerve and press it against the μcoil (see supplementary information S8). This design could potentially solve this challenge caused by changes in the orientation of the μcoil after implantation. The MagPen is a single μcoil prototype. In the future, the spatial specificity for neural activation by the MagPen could be further enhanced by designing arrays of μcoils [52].

The dose-response relationship was measured for seven rats independently. Interestingly, in two rats, we observed the activation of different muscles depending on the waveform used. In these experiments, low frequency (high duration) micromagnetic stimuli induced dorsiflexion of the foot (see supplementary video SV7) while high frequency (low duration) micromagnetic stimuli generated knee flexion (see supplementary video SV8). Most frequencies on the dose-response chart in figure 8(a) generated dorsiflexion. It would be of interest to show a veterinarian the experimental set-up to judge which muscles are being activated. We estimate where to place the EMG needle and which muscles are activated based on an anatomical atlas of the leg. The location of each is correlated to where the MagPen is stimulating on the sciatic nerve and likely to where we cut down during surgery. Based on the orientation of the μcoil with respect to the stimulation site on the nerve, the pathway for dorsiflexion would primarily be activated. Another interesting experiment that could be performed with the neuromodulation technique is to demonstrate fascicle-specific activation in the nerve. However, this process is extremely challenging to demonstrate on a rat sciatic nerve because of the existing difficulty of orienting the μcoil to see activation and targeting a specific fascicle to stimulate would be even more difficult. Such an experiment will likely need to be performed on a frog sciatic nerve (a bigger nerve).

5. Conclusions

This *in vivo* experimental work reports the activation of the rat right sciatic nerve using sub-mm-sized μcoils by tracking right hind limb motion. For the first time, we experimentally report the dose-response relationship for μMS using the MagPen prototype. The orientation dependence of the nerve with respect to the μcoils was studied. The resulting relationship between orientation and stimulus waveform was predicted directly from Faraday's laws of electromagnetic induction. While μMS resulted in similar responses as electrical stimulation, there are important differences. First, the μcoils do not have an electrochemical interface, so they may not be as sensitive to biofouling as electrodes. Second, magnetic fields fall off faster than electric fields, so μcoils may have much higher specificity than monopolar, or even bipolar, electrodes. Third, the MagPen induces electric fields in the tissue, and the strength of the field increases with frequency for the same amplitude of current driving the μcoil. This work demonstrates that μMS using sub-mm-sized μcoils can be used as an

alternative to the electrode technology for focal neural stimulation.

Data availability statement

All data that support the findings of this study are included within the article (and any supplementary files).

Acknowledgments

This study was financially supported by the Minnesota Partnership for Biotechnology and Medical Genomics under award number ML2020. Chap 64. Art I, Sec 1. 4. R S acknowledges the 3 year College of Science and Engineering (CSE) Fellowship awarded by the University of Minnesota, Twin Cities. Research reported in this publication was supported by the University of Minnesota's MnDRIVE (Minnesota's Discovery, Research and Innovation Economy) initiative. The authors would also like to thank Dr Winfried A Raabe, M D from the Department of Neurosurgery (UMN) and Kendall H Lee, M D, PhD, Charles D Blaha, PhD, and Yoonbae Oh, PhD from the Mayo Clinic, Rochester, MN for useful discussions. Portions of this work were conducted in the Minnesota Nano Center (MNC), which is supported by the National Science Foundation through the National Nano Coordinated Infrastructure Network (NNCI) under Award Number ECCS-2025124. J P W and R S also thank the Robert Hartmann Endowed Chair for support.

Conflict of interest

The authors declare no conflicts of interest.

ORCID iDs

Renata Saha https://orcid.org/0000-0002-0389-0083
Zachary Sanger https://orcid.org/0000-0003-2144-1895
Robert P Bloom https://orcid.org/0000-0002-7781-5270
Onri J Benally https://orcid.org/0000-0002-8391-9105
Kai Wu https://orcid.org/0000-0002-9444-6112
Denis Tonini https://orcid.org/0000-0001-5121-5544
Walter C Low https://orcid.org/0000-0001-8593-0175
Susan A Keirstead https://orcid.org/0000-0002-7610-678X
Theoden I Netoff https://orcid.org/0000-0002-0115-1930
Jian-Ping Wang https://orcid.org/0000-0003-2815-6624

References

[1] Gybels J and Kupers R 1987 Central and peripheral electrical stimulation of the nervous system in the treatment of chronic pain *Pain* pp 64–75
[2] Kapural L, Gupta M, Paicius R, Strodtbeck W, Vorenkamp K E, Gilmore C, Gliner B, Rotte A, Subbaroyan J and Province-Azalde R 2020 Treatment of chronic abdominal pain with 10 kHz spinal cord stimulation: safety and efficacy results from a 12 month prospective, multicenter, feasibility study *Clin. Transl. Gastroenterol.* **11** e00133
[3] Hofmeister M, Memedovich A, Brown S, Saini M, Dowsett L E, Lorenzetti D L, McCarron T L, MacKean G and Clement F 2020 Effectiveness of neurostimulation technologies for the management of chronic pain: a systematic review *Neuromodulation* **23** 150–7
[4] Klinger N and Mittal S 2018 Deep brain stimulation for seizure control in drug-resistant epilepsy *Neurosurg. Focus* **45** E4
[5] Salanova V 2018 Deep brain stimulation for epilepsy *Epilepsy Behav.* **88** 21–24
[6] Little S and Brown P 2020 Debugging adaptive deep brain stimulation for Parkinson's disease *Mov. Disorders* **35** 555–61
[7] Kaminska M, Perides S, Lumsden D E, Nakou V, Selway R, Ashkan K and Lin J-P 2017 Complications of deep brain stimulation (DBS) for dystonia in children–the challenges and 10 year experience in a large paediatric cohort *Eur. J. Paediatr. Neurol.* **21** 168–75
[8] Weiland J D, Cho A K and Humayun M S 2011 Retinal prostheses: current clinical results and future needs *Ophthalmology* **118** 2227–37
[9] Tong W, Meffin H, Garrett D J and Ibbotson M R 2020 Stimulation strategies for improving the resolution of retinal prostheses *Front. Neurosci.* **14** 262
[10] Gildenberg P L 2006 History of electrical neuromodulation for chronic pain *Pain Med.* **7** S7–S13
[11] Fritsch G 1870 Uber die elektrische Erregbarkeit des Grosshirns *Arch Anat Physiol.* **37** 300–32
[12] Greenblatt S H 1997 *A History of Neurosurgery: In Its Scientific and Professional Contexts* (Thieme) (available at: https://books.google.com/books/about/A_History_of_Neurosurgery.html?id=QMNfYE8XVXcC)
[13] Gildenberg P L 2006 History of electrical neuromodulation for chronic pain *Pain Med.* **7** S7–13
[14] Johnson M I 2021 Resolving long-standing uncertainty about the clinical efficacy of transcutaneous electrical nerve stimulation (TENS) to relieve pain: a comprehensive review of factors influencing outcome *Medicina* **57** 378
[15] Okonkwo U P, Ibeneme S C, Ihegihu E Y, Egwuonwu A V, Ezema I C, Maruf A F, Okoye E C, Ibikunle O P and Ezeukwu A O 2018 Effects of transcutaneous electrical nerve stimulation in the Management of Post-Injection Sciatic Pain in a non-randomized controlled clinical trial in Nnewi, Nigeria *BMC Complement. Altern. Med.* **18** 1–11
[16] El-sayed A G, White P F, Ahmed H E, Hamza M A, Craig W F and Noe C E 1999 Percutaneous electrical nerve stimulation: an alternative to TENS in the management of sciatica *Pain* **83** 193–9
[17] Ilfeld B M, Gabriel R A, Said E T, Monahan A M, Sztain J F, Abramson W B, Khatibi B, Finneran J J, Jaeger P T and Schwartz A K 2018 Ultrasound-guided percutaneous peripheral nerve stimulation: neuromodulation of the sciatic nerve for postoperative analgesia following ambulatory foot surgery, a proof-of-concept study *Reg. Anesth. Pain Med.* **43** 580–9
[18] Larson C E and Meng E 2020 A review for the peripheral nerve interface designer *J. Neurosci. Methods* **332** 108523
[19] Boretius T, Badia J, Pascual-Font A, Schuettler M, Navarro X, Yoshida K and Stieglitz T 2010 A transverse intrafascicular multichannel electrode (TIME) to interface with the peripheral nerve *Biosens. Bioelectron.* **26** 62–69

[20] Badia J, Boretius T, Andreu D, Azevedo-Coste C, Stieglitz T and Navarro X 2011 Comparative analysis of transverse intrafascicular multichannel, longitudinal intrafascicular and multipolar cuff electrodes for the selective stimulation of nerve fascicles *J. Neural Eng.* **8** 036023
[21] Sharma A, Rieth L, Tathireddy P, Harrison R, Oppermann H, Klein M, Töpper M, Jung E, Normann R and Clark G 2012 Evaluation of the packaging and encapsulation reliability in fully integrated, fully wireless 100 channel Utah slant electrode array (USEA): implications for long term functionality *Sens. Actuators* A **188** 167–72
[22] Xu J and Lee H 2020 Anti-biofouling strategies for long-term continuous use of implantable biosensors *Chemosensors* **8** 66
[23] Seaton B T, Hill D F, Cowen S L and Heien M L 2020 Mitigating the effects of electrode biofouling-induced impedance for improved long-term electrochemical measurements *in vivo Anal. Chem.* **92** 6334–40
[24] Bonmassar G and Serano P 2020 MRI-induced heating of coils for microscopic magnetic stimulation at 1.5 tesla: an initial study *Front. Hum. Neurosci.* **14** 53
[25] Saha R, Faramarzi S, Bloom R, Benally O J, Wu K, Di Girolamo A, Tonini D, Keirstead S A, Low W C and Netoff T 2022 Strength-frequency curve for micromagnetic neurostimulation through excitatory postsynaptic potentials (EPSPs) on rat hippocampal neurons and numerical modeling of magnetic microcoil (μcoil) *J. Neural Eng.* **19** 016018
[26] Bonmassar G, Lee S W, Freeman D K, Polasek M, Fried S I and Gale J T 2012 Microscopic magnetic stimulation of neural tissue *Nat. Commun.* **3** 921
[27] Minusa S, Osanai H and Tateno T 2017 Micromagnetic stimulation of the mouse auditory cortex *in vivo* using an implantable solenoid system *IEEE Trans. Biomed. Eng.* **65** 1301–10
[28] Lee S W, Fallegger F, Casse B D and Fried S I 2016 Implantable microcoils for intracortical magnetic stimulation *Sci. Adv.* **2** e1600889
[29] Colella M, Laher R M, Press D Z, McIlduff C E, Rutkove S B, Pascual-Leone A, Apollonio F, Liberti M and Bonmassar G 2019 Ultra-focal magnetic stimulation using a μTMS coil: a computational study *2019 41st Annual Int. Conf. of the IEEE Engineering in Medicine and Biology Society (EMBC)* (IEEE) pp 3987–90
[30] Sarreal R R S, Blake D T and Bhatti P T 2022 Development and characterization of a micromagnetic alternative to cochlear implant electrode arrays *IEEE Trans. Neural Syst. Rehabil. Eng.* **30** 2116–25
[31] Lee S W and Fried S I 2016 Enhanced control of cortical pyramidal neurons with micromagnetic stimulation *IEEE Trans. Neural Syst. Rehabil. Eng.* **25** 1375–86
[32] Ye H and Barrett L 2021 Somatic inhibition by microscopic magnetic stimulation *Sci. Rep.* **11** 1–18
[33] Skach J, Conway C, Barrett L and Ye H 2020 Axonal blockage with microscopic magnetic stimulation *Sci. Rep.* **10** 1–18
[34] Kagan Z B, RamRakhyani A K, Lazzi G, Normann R A and Warren D J 2016 *In vivo* magnetic stimulation of rat sciatic nerve with centimeter-and millimeter-scale solenoid coils *IEEE Trans. Neural Syst. Rehabil. Eng.* **24** 1138–47
[35] Kim T, Kadji H, Whalen A J, Ashourvan A, Freeman E, Fried S I, Tadigadapa S and Schiff S J 2022 Thermal effects on neurons during stimulation of the brain *J. Neural Eng.* **19** 056029
[36] Kim S, Normann R A, Harrison R and Solzbacher F 2006 Preliminary study of the thermal impact of a microelectrode array implanted in the brain *2006 Int. Conf. of the IEEE Engineering in Medicine and Biology Society* (IEEE) pp 2986–9
[37] Kim S, Tathireddy P, Normann R A and Solzbacher F 2007 *In vitro* and *in vivo* study of temperature increases in the brain due to a neural implant *2007 3rd Int. IEEE/EMBS Conf. on Neural Engineering* (IEEE) pp 163–6
[38] Jeong H, Cho A, Ay I and Bonmassar G 2022 Short-pulsed micro-magnetic stimulation of the vagus nerve *Front. Physiol.* **13** 938101
[39] Moyer J R Jr and Brown T H 1998 Methods for whole-cell recording from visually preselected neurons of perirhinal cortex in brain slices from young and aging rats *J. Neurosci. Methods* **86** 35–54
[40] Kagan Z B, Mize J T, Kosta P, Lazzi G, Normann R A and Warren D J 2019 Reduced heat generation during magnetic stimulation of rat sciatic nerve using current waveform truncation *IEEE Trans. Neural Syst. Rehabil. Eng.* **27** 937–46
[41] Park H-J, Seol J H, Ku J and Kim S 2015 Computational study on the thermal effects of implantable magnetic stimulation based on planar coils *IEEE Trans. Biomed. Eng.* **63** 158–67
[42] Oh Y, Heien M L, Park C, Kang Y M, Kim J, Boschen S L, Shin H, Cho H U, Blaha C D and Bennet K E 2018 Tracking tonic dopamine levels *in vivo* using multiple cyclic square wave voltammetry *Biosens. Bioelectron.* **121** 174–82
[43] Khalifa A, Zaeimbashi M, Zhou T X, Abrishami S M, Sun N, Park S, Šumarac T, Qu J, Zohar I and Yacoby A 2021 The development of microfabricated solenoids with magnetic cores for micromagnetic neural stimulation *Microsyst. Nanoeng.* **7** 1–10
[44] Wagner T, Gangitano M, Romero R, Théoret H, Kobayashi M, Anschel D, Ives J, Cuffin N, Schomer D and Pascual-Leone A 2004 Intracranial measurement of current densities induced by transcranial magnetic stimulation in the human brain *Neurosci. Lett.* **354** 91–94
[45] Wagner T A, Zahn M, Grodzinsky A J and Pascual-Leone A 2004 Three-dimensional head model simulation of transcranial magnetic stimulation *IEEE Trans. Biomed. Eng.* **51** 1586–98
[46] Golestanirad L, Mattes M, Mosig J R and Pollo C 2010 Effect of model accuracy on the result of computed current densities in the simulation of transcranial magnetic stimulation *IEEE Trans. Magn.* **46** 4046–51
[47] Martyanov A S and Neustroyev N I 2014 ANSYS Maxwell software for electromagnetic field calculations *East. Eur. Sci. J.* **5**
[48] Ren Z 2002 T-/spl omega/formulation for eddy-current problems in multiply connected regions *IEEE Trans. Magn.* **38** 557–60
[49] Golestanirad L, Gale J T, Manzoor N F, Park H-J, Glait L, Haer F, Kaltenbach J A and Bonmassar G 2018 Solenoidal micromagnetic stimulation enables activation of axons with specific orientation *Front. Physiol.* **9** 724
[50] Park H and Kim S 2013 Computational study on thermal effects of coil-based implantable magnetic stimulation using finite element analysis *2013 6th Int. IEEE/EMBS Conf. on Neural Engineering (NER)* (IEEE) pp 1497–500
[51] Erhardt J B, Fuhrer E, Gruschke O G, Leupold J, Wapler M C, Hennig J, Stieglitz T and Korvink J G 2018 Should patients with brain implants undergo MRI? *J. Neural Eng.* **15** 041002
[52] Minusa S, Muramatsu S, Osanai H and Tateno T 2019 A multichannel magnetic stimulation system using submillimeter-sized coils: system development and experimental application to rodent brain *in vivo J. Neural Eng.* **16** 066014